nature biotechnology

Self-sufficient control of urate homeostasis in mice by a synthetic circuit

Christian Kemmer[1], Marc Gitzinger[1], Marie Daoud-El Baba[2], Valentin Djonov[3], Jörg Stelling[1,4] & Martin Fussenegger[1]

© 2010 Nature America, Inc. All rights reserved.

Synthetic biology has shown that the metabolic behavior of mammalian cells can be altered by genetic devices such as epigenetic and hysteretic switches[1,2], timers and oscillators[3,4], biocomputers[5], hormone systems[6] and heterologous metabolic shunts[7]. To explore the potential of such devices for therapeutic strategies, we designed a synthetic mammalian circuit to maintain uric acid homeostasis in the bloodstream, disturbance of which is associated with tumor lysis syndrome and gout[8,9]. This synthetic device consists of a modified *Deinococcus radiodurans*-derived protein that senses uric acids levels and triggers dose-dependent derepression of a secretion-engineered *Aspergillus flavus* urate oxidase that eliminates uric acid. In urate oxidase–deficient mice, which develop acute hyperuricemia, the synthetic circuit decreased blood urate concentration to stable sub-pathologic levels in a dose-dependent manner and reduced uric acid crystal deposits in the kidney. Synthetic gene-network devices providing self-sufficient control of pathologic metabolites represent molecular prostheses, which may foster advances in future gene- and cell-based therapies.

State-of-the-art treatment of metabolic disorders consists of small-molecule drug-based interventions to fix out-of-control physiology. However, the daily dosing of drug-based therapies is rather empiric, which may result in undesired side effects. Thus, prosthetic gene-network devices integrated into cells and functionally connected to their metabolism could sense and correct metabolic disturbances as they develop by triggering therapeutic responses in a self-sufficient manner.

As a model system, we explored the potential of a mammalian synthetic circuit for maintaining homeostasis of urate in the bloodstream. Urate is the end-product of purine metabolism, and its homeostasis may be disturbed by genetic predisposition, environmental factors, therapeutic interventions and nutritional imbalances, leading to hyperuricemia. Excess urate favors the formation of pathologic monosodium urate and uric acid crystals in the joints, kidney and subcutaneous tissues, which can trigger a variety of urate-associated pathologies, including the tumor lysis syndrome and gout[9–11].

We began by engineering a synthetic circuit able to sense and respond to uric acid. The circuit uses a bacterial transcriptional repressor (HucR) that binds a DNA sequence motif (hucO) in the absence of uric acid. When uric acid is present, HucR dissociates from DNA, thereby allowing expression of a downstream gene.

HucR and hucO were cloned from *Deinococcus radiodurans* R1 based on molecular insight into this bacteria's remarkable ability to withstand DNA damage caused by ultraviolet radiation and oxidative stress[12]. Recently, a hypothetical uricase regulator (HucR) was identified in *D. radiodurans* and was suggested to play a critical role in the cellular response to oxidative stress[13]. Like mammals, *D. radiodurans* takes advantage of the radical-scavenging activity of uric acid, yet needs to control uric acid levels to prevent crystallization. HucR was shown to bind to a dyad-symmetrical operator site (hucO) in the intergenic region of divergently transcribed *hucR* and a gene encoding a putative uricase, suggesting that both genes are co-repressed by HucR, unless excessive uric acid levels trigger the release of HucR from hucO and induce uricase expression[13,14]. Taken together, these prior observations suggested that HucR and hucO could be used as building blocks in a uric acid–responsive expression network.

The uric acid–responsive expression network (UREX) required engineering HucR and hucO for optimal performance in mammalian cells (**Supplementary Table 1**). The HucR start codon was modified (GTG→ATG) and fused to a Kozak consensus sequence for maximum expression of the repressor protein in mammalian cells (mHucR). mHucR was engineered to be a stronger repressor by fusing it to the C terminus of the Krueppel-associated box (KRAB) protein domain[15]. Notably, fusing mHucR to the N terminus abolished the urate-responsiveness of mHucR (data not shown). The resulting repressor is a chimeric mammalian urate-dependent transsilencer (mUTS). To engineer a promoter that strongly drives expression of a target gene in the presence of uric acid, yet has low basal expression levels in the absence of uric acid, we placed eight tandem hucO modules downstream of a simian virus 40 promoter (P_{SV40}-$hucO_8$, referred hereafter as P_{UREX8}) (**Fig. 1a**). P_{UREX8} was chosen as part of the uric acid sensor circuit because it provided the tightest repression in preliminary tests (for a detailed and quantitative evaluation of alternative promoter configurations, see below).

[1]Department of Biosystems Science and Engineering, ETH Zurich, Basel, Switzerland. [2]Institut Universitaire de Technologie, IUTA, Département Génie Biologique, Villeurbanne Cedex, France. [3]Département de Médecine, Université de Fribourg, Fribourg, Switzerland. [4]Swiss Institute of Bioinformatics, ETH Zurich, Zurich, Switzerland. Correspondence should be addressed to M.F. (fussenegger@bsse.ethz.ch) or J.S. (joerg.stelling@bsse.ethz.ch).

Received 1 February; accepted 19 February; published online 28 March 2010; doi:10.1038/nbt.1617

We characterized the performance of P_{UREX8} by cloning it upstream of a reporter gene encoding SEAP (human placental secreted alkaline phosphatase), which is assayed in the culture supernatant. In the absence of uric acid, mUTS binds $hucO_8$ and silences transcription from P_{UREX8} (**Fig. 1b**). However, in the presence of uric acid, mUTS is released from $hucO_8$ thereby inducing SEAP expression. Co-transfection of a vector constitutively expressing mUTS (pCK25) and the vector with SEAP controlled by P_{UREX8} (pCK9) into human cervical adenocarcinoma cells (HeLa), human embryonic kidney cells (HEK-293) and human fibrosarcoma cells (HT-1080) grown in medium free of uric acid showed that mUTS bound and silenced P_{UREX8}-driven SEAP expression up to 98% (**Fig. 1c**), reaching a tightness which was previously only achieved by more complex transcription-translation networks[16]. Constitutive expression of mUTS was driven by the human elongation factor 1α promoter ($P_{hEF1\alpha}$). Addition of 5 mM uric acid to transfected cultures triggered the release of mUTS from $hucO_8$ and derepressed SEAP expression (**Fig. 1d–f**).

To increase the sensitivity of the UREX circuit to uric acid, we co-transfected it into cells with a third plasmid that expressed the human urate-anion transporter URAT1, which is naturally involved in renal urate clearance and maintenance of uric acid homeostasis[17,18]. The transporter's urate-uptake capacity is expected to increase intracellular uric acid levels and consequently amplify UREX sensitivity. Transfecting a constitutive URAT1 expression vector (pURAT1) into HeLa, HEK-293 and HT-1080 cells engineered for UREX-controlled SEAP expression resulted in considerably higher SEAP levels (**Fig. 1d–f**) compared with URAT1-free cells or with cells that constitutively expressed a control anion transporter OAT2 (human organic anion transporter 2), which is unrelated to uric acid transport. The expression of either endogenous or transgenic URAT1 and OAT2 was determined by semiquantitative RT-PCR and demonstrated that neither HeLa, HEK-293 nor HT-1080 wild-type cells express endogenous URAT1 or OAT2 (**Supplementary Fig. 1** and **Supplementary Table 2**).

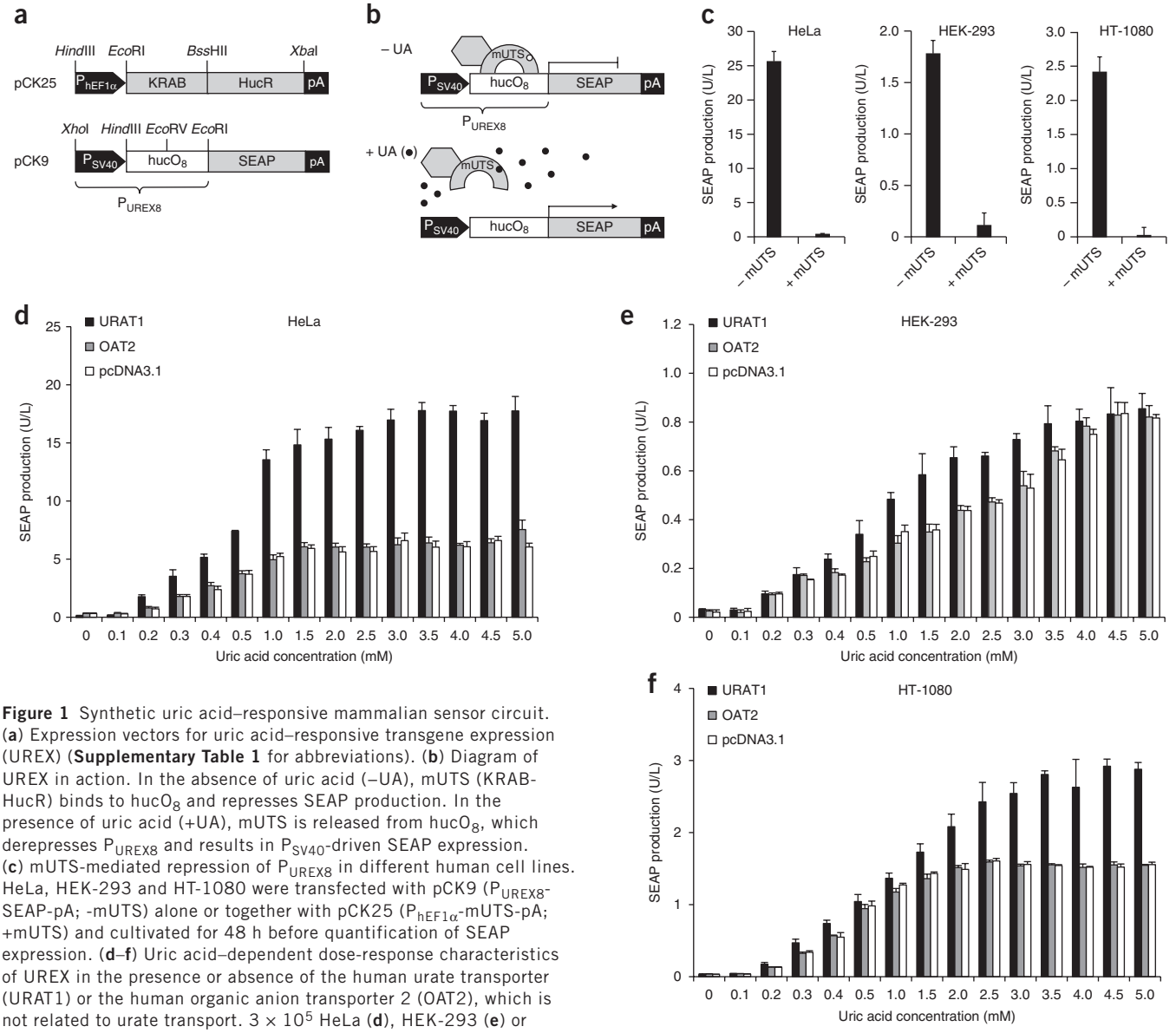

Figure 1 Synthetic uric acid–responsive mammalian sensor circuit. (**a**) Expression vectors for uric acid–responsive transgene expression (UREX) (**Supplementary Table 1** for abbreviations). (**b**) Diagram of UREX in action. In the absence of uric acid (–UA), mUTS (KRAB-HucR) binds to $hucO_8$ and represses SEAP production. In the presence of uric acid (+UA), mUTS is released from $hucO_8$, which derepresses P_{UREX8} and results in P_{SV40}-driven SEAP expression. (**c**) mUTS-mediated repression of P_{UREX8} in different human cell lines. HeLa, HEK-293 and HT-1080 were transfected with pCK9 (P_{UREX8}-SEAP-pA; -mUTS) alone or together with pCK25 ($P_{hEF1\alpha}$-mUTS-pA; +mUTS) and cultivated for 48 h before quantification of SEAP expression. (**d–f**) Uric acid–dependent dose-response characteristics of UREX in the presence or absence of the human urate transporter (URAT1) or the human organic anion transporter 2 (OAT2), which is not related to urate transport. 3×10^5 HeLa (**d**), HEK-293 (**e**) or HT-1080 (**f**) were co-transfected with the UREX sensor plasmids pCK9 and pCK25 (**Fig. 1a**) and either pURAT1 (P_{hCMV}-URAT1-pA), pOAT2 (P_{hCMV}-OAT2-pA) or the isogenic control vector pcDNA3.1. The transfected populations were cultivated in medium supplemented with different uric acid concentrations and resulting SEAP levels were profiled after 48 h.

© 2010 Nature America, Inc. All rights reserved.

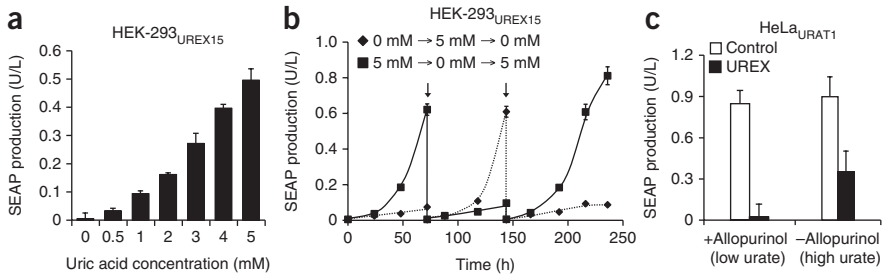

Figure 2 Validation of UREX-controlled SEAP expression in transgenic HEK-293 and urate oxidase–deficient mice. (**a**) Uric acid–based dose response profile of the triple-transgenic HEK-293$_{UREX15}$ cell line stably engineered for UREX-controlled SEAP and constitutive URAT1 expression. 5×10^4 HEK-293$_{UREX15}$ cells were cultivated in the presence of different uric acid concentrations and SEAP levels were quantified in the culture supernatant after 72 h. (**b**) Reversibility of the UREX-based uric acid sensor circuit. 2×10^5 HEK-293$_{UREX15}$ cells were cultivated for 10 d while uric acid concentrations were alternated from 0–5 mM every 72 h (arrows). (**c**) HeLa$_{URAT1}$ cells engineered for UREX-controlled SEAP expression were microencapsulated in coherent alginate-poly-L-lysine-alginate microcapsules and intraperitoneally injected (2×10^6 cells per mouse, 200 cells/capsule) into *uox*$^{-/-}$ mice that had received 150 µg/ml (wt/vol) of the hyperuricemia therapeutic allopurinol (+allopurinol) in their drinking water to reduce urate levels (UREX) or untreated *uox*$^{-/-}$ mice exhibiting pathologic urate levels (–allopurinol). Control implants contained cells transgenic for constitutive SEAP expression (control). SEAP levels were profiled in the serum of the animals 72 h after cell implantation.

HeLa cells were particularly more sensitive within the urate range typically found in the human blood (200–500 µM) (**Fig. 1d–f**).

To characterize adjustability and long-term reversibility of the mammalian uric acid sensor system, we constructed the stable human cell line HEK-293$_{UREX15}$ that is triple-transgenic for UREX-controlled SEAP and constitutive URAT1 expression. SEAP expression of HEK-293$_{UREX15}$ could be precisely adjusted and showed a progressive increase in response to escalating concentrations of uric acid (**Fig. 2a**). Reversibility of UREX-controlled SEAP production was assessed by cultivating HEK-293$_{UREX15}$ for 10 d while alternating uric acid concentrations from 0 mM to 5 mM every 72 h. UREX control was completely reversible and could be reset at any time without showing any expression memory effect on SEAP production (**Fig. 2b**). Indeed, 72 h after intraperitoneal implantation of microencapsulated cells engineered for URAT1 and UREX-controlled SEAP expression into urate oxidase-deficient (*uox*$^{-/-}$) mice that were developing hyperuricemia with human-like symptoms[19], the synthetic urate sensor circuit was sufficiently sensitive to discriminate between mice developing hyperuricemia (high urate levels (23.1 ± 5.6 (s.d.) mg/dl); 0.35 ± 0.15 (s.d.) U/L SEAP) and animals that received the licensed urate-reducing arthritis therapeutic allopurinol (Zyloprim) in their drinking water (low urate levels (7.8 ± 3.1 (s.d.) mg/dl); 0.02 ± 0.10 (s.d.) U/L SEAP) (**Fig. 2c**). Control mice treated with cells constitutively producing SEAP showed unaltered SEAP expression in the presence (low urate levels; 0.85 ± 0.10 (s.d.) U/L SEAP) or absence (high urate levels; 0.90 ± 0.15 (s.d.) U/L SEAP) of allopurinol. Taken together, these results suggest that the precise and robust uric acid sensor UREX may be suitable for therapeutic control of this pathologic metabolite.

For feedback-controlled reduction of uric acid levels in an autonomous and self-sufficient manner, the uric acid sensor circuit must be linked to expression of a uricase/urate oxidase (Uox) which converts urate to the more soluble and renally secretable allantoin[20]. We therefore optimized the codons of the cofactor-independent *Aspergillus flavus* uricase for expression in mammalian cells obtaining mUox.

mUox reduced uric acid (0.5 mM) in the culture medium when constitutively expressed (P$_{UREX8}$-mUox-pA, referred to as pCK67) or controlled by mUTS (pCK67 with pCK25, which constitutively expresses mUTS) (**Fig. 3a**). Urate reduction was more efficient when mUox was engineered for mammalian cell–based secretion by in-frame fusion to an immunoglobulin-derived secretion signal[21] (SS$_{Igk}$). This optimized uricase, which is referred to as smUox, was used in further studies and was expressed on plasmid pCK65 (P$_{UREX8}$-SS$_{Igk}$-mUox-pA).

The dynamics of UREX-controlled uric acid metabolism were profiled during a 120-h cultivation of HeLa$_{URAT1}$ (a HeLa-derived cell line transgenic for constitutive URAT1 expression) engineered for constitutive mUTS and P$_{UREX8}$-driven smUox expression (**Fig. 3b**). Isogenic HeLa$_{URAT1}$ control cells that constitutively expressed smUox (without mUTS co-expression) cleared uric acid from the medium. In contrast, the uric acid levels of cell cultures harboring the synthetic UREX-smUox control circuit leveled out at 0.14 mM (a concentration suggested to support oxidative-stress protection in a physiologic context), even when exposed to different starting uric acid concentrations. These results indicate that uric acid levels have fallen below a threshold concentration that was no longer able to induce UREX control and trigger further urate oxidation (**Fig. 3b**). The uric acid homeostasis level of 0.14 mM was consistently reached even when the UREX-based control device was challenged with a second dose of uric acid after 72 h (**Fig. 3c**). Overall, these data confirm self-sufficient feedback control of uric acid levels by UREX-smUox and suggest that this synthetic circuit could reduce pathologic urate levels into a physiologic window in an auto-controlled manner.

To further elucidate how the UREX system and its key design features, such as the number of hucO sites in P$_{UREX}$, would influence uric acid homeostasis *in vivo*, we established a dynamic mathematical model based on ordinary differential equations. Briefly, we developed an eight-state model that describes all relevant processes such as (controlled) gene expression, transport and other enzyme-catalyzed reactions. Model parameters were constrained by literature data and further parameter estimation using part of the experimental data for the UREX system in HeLa cells. We validated the model with independent predictions, and obtained good matches between simulation results and experimental data in both scenarios. In addition, changes in a subset of cell line–specific model parameters allowed us to quantitatively capture UREX dose responses in HEK-293 and HT-1080 cells as well (**Supplementary Results**, **Supplementary Figs. 2–7** and **Supplementary Tables 3** and **4**).

To predict the behavior after encapsulation of the HeLa$_{URAT1}$-based system in mice, we initially used a simplified mathematical model where the implant and the cells inside are in a flow with constant influx and identical outflux with respect to the mouse body, such that the liquid volume is constant. This situation corresponds to the setup of a chemostat with cell retention for different constant dilution rates and input uric acid concentrations. The model predictions show that, for large ranges of these parameters, the system will achieve a desirable steady-state uric acid output concentration in the physiological range. Moreover, with eight HucR binding sites per P$_{UREX}$, the system will be rather insensitive to variations in uric acid

© 2010 Nature America, Inc. All rights reserved.

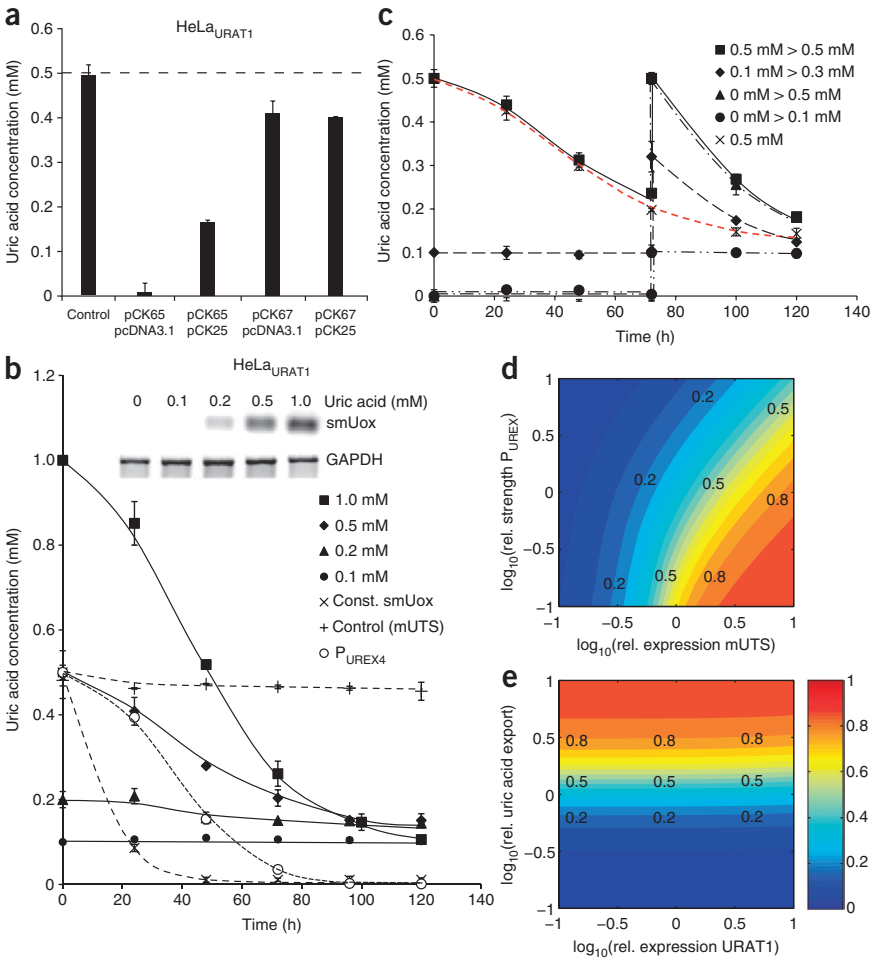

Figure 3 Functional characterization of an engineered mammalian *A. flavus*–derived urate oxidase. (**a**) Profiling of urate reduction mediated by constitutive or UREX-controlled expression of an intracellular (mUox) or secretion-engineered (smUox) urate oxidase variant. 2×10^5 HeLa$_{URAT1}$ cells were co-transfected with either pCK65 and isogenic control vector pcDNA3.1, pCK65 and pCK25, pCK67 and pcDNA3.1, or pCK67 and pCK25. The cells were cultivated for 72 h with 0.5 mM uric acid before uric acid levels were determined in the culture supernatant. (**b**) Uric acid degradation profiles of UREX-controlled smUox expression. 2×10^5 HeLa$_{URAT1}$ cells engineered for UREX-controlled smUox expression (solid lines) were cultivated in medium containing starting uric acid concentrations of either 0.1, 0.2, 0.5 or 1 mM and uric acid reduction kinetics were profiled for 120 h. Control experiments show 2×10^5 HeLa$_{URAT1}$ engineered for constitutive smUox or mUTS expression (dashed lines). The upper panel shows smUox and GAPDH (control) transcript levels profiled 24 h after induction. (**c**) Uric acid homeostasis. 2×10^5 HeLa$_{URAT1}$ cells engineered for UREX-controlled smUox expression were cultivated in medium containing starting concentrations of 0, 0.1 or 0.5 mM uric acid. After 72 h the cultures received a second dose of uric acid (0.1, 0.3, 0.5 mM) after which the UREX-based control device again adjusted uric acid concentrations to the homeostasis level (dashed red line, 0.5 mM uric acid profile of **Fig. 3b**). (**d**,**e**) Model predictions for uric acid homeostasis using a physiological model. Steady-state values of uric acid concentration obtained by simulating the interplay of UREX circuit in HeLa$_{URAT1}$ cells and of body cells connected by a fluid flow (**Supplementary Results**). Contour plots of steady-state extracellular urate concentration as a function of relative mUTS expression and of relative P$_{UREX}$ promoter strength (**d**), and as a function of relative URAT1 expression and of maximal uric acid export rate (**e**), respectively. Colors indicate concentrations according to the color bar in **e**; see also labels, values in mM.

© 2010 Nature America, Inc. All rights reserved.

input, but substantially fewer operator sites will result in unphysiologically low levels because of too-leaky promoter characteristics (**Supplementary Results** and **Supplementary Fig. 8**).

We tested these predictions by developing a more detailed promoter model and by experimentally constructing UREX circuits with P$_{UREX}$ variants harboring fewer than eight binding sites. Both approaches showed very good quantitative agreement with the earlier predictions. An example for UREX-controlled dynamics with P$_{UREX4}$ is shown in **Figure 3b** (**Supplementary Results**, **Supplementary Figs. 9–12** and **Supplementary Table 5**). Finally, we embedded the model into a more realistic physiological setting by conceptually splitting the mouse into two compartments, one containing the UREX implant and the other one consisting of the rest of the animal, respectively. For broad ranges of parameter values this model confirmed uric acid homeostasis (**Supplementary Results** and **Supplementary Fig. 13**). In addition, it allowed for detailed predictions of possibilities for fine-tuning the circuit. For instance, the model predicts that variation of mUTS levels is more effective in adjusting the circuit than replacing the promoter in P$_{UREX}$ (**Fig. 3d**). Surprisingly, the model reveals that manipulation of uric acid export is more promising than adjustment of URAT1 expression, to which the system is not sensitive at all (**Fig. 3e**). Hence, the model predictions further reinforce the potential use of the synthetic circuit for uric acid homeostasis in pathological conditions, and they suggest key design features of the circuit.

When urate oxidase–deficient *uox*$^{-/-}$ mice were treated with cell implants expressing UREX-controlled smUox, urate levels in serum and in urine dropped to concentrations reached by standard allopurinol therapy. In contrast, control animals (e.g., HeLa$_{URAT1}$ cell implants, no allopurinol) accumulated urate and developed acute hyperuricemia in the absence of allopurinol with acute uric acid crystal deposition in renal tubules resembling those of the tumor lysis syndrome in humans[19] (**Fig. 4a**,**b**). Histologic analysis of H&E-stained kidney sections from all treatment groups confirmed that UREX-smUox-based therapeutic cell implants were able to considerably reduce uric acid crystal deposits in the proximal tubules (**Fig. 4c–f**).

Gout is the most common inflammatory arthritis, affecting >1% of the human population in industrialized countries. Clinical manifestations, which result from monosodium urate crystal deposition, include acute gouty arthritis, chronic gouty arthropathy, tophi, renal dysfunction and urolithiasis[9,11]. Owing to a urate oxidase deficiency, urate blood levels of humans are up to 50 times higher than in other mammals, which increases the risk of developing hyperuricemic diseases[11,17]. Uric acid has been suggested to be a free radical scavenger that may protect living systems from lipid peroxidation, DNA

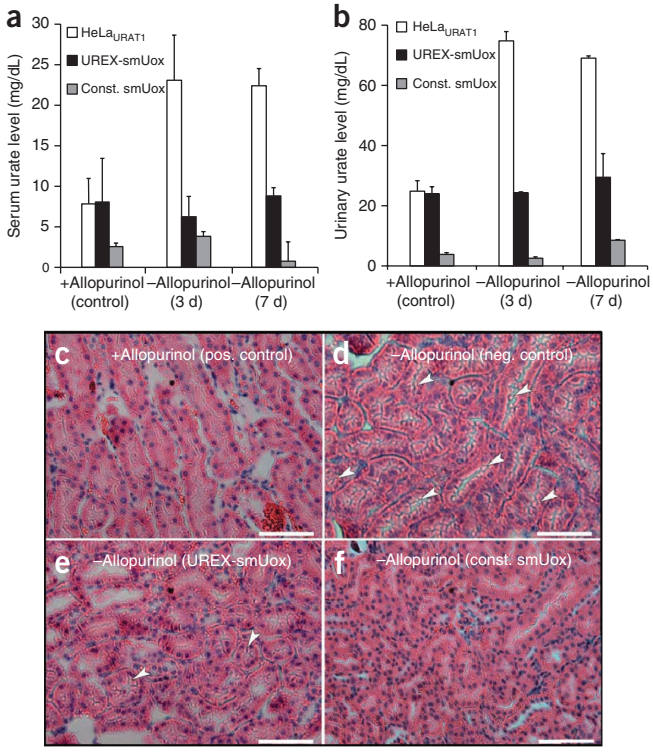

Figure 4 UREX-controlled smUox-mediated reduction of pathologic urate levels in mice. Microencapsulated HeLa$_{URAT1}$ cells engineered for UREX-controlled smUox expression were intraperitoneally implanted (2×10^6 cells per mouse) into untreated *uox*$^{-/-}$ mice exhibiting pathologic urate levels or into *uox*$^{-/-}$ mice having received 150 µg/ml (wt/vol) of the hyperuricemia therapeutic allopurinol in their drinking water (UREX-smUox) (control). Control implants contained parental HeLa$_{URAT1}$. (**a**,**b**) Urate levels were profiled in serum (**a**) and urine (collected for 24 h) (**b**) of the animals 3 and 7 d after cell implantation. (**c**–**f**) Tissue sections showing anisotropic uric acid crystals (arrow) in the kidneys of *uox*$^{-/-}$ mice receiving 150 µg/ml (wt/vol) allopurinol (positive control) (**c**), phosphate-buffered saline (negative control) (**d**), implants with HeLa$_{URAT1}$ engineered for UREX-controlled smUox expression (**e**) and implants with HeLa$_{URAT1}$ engineered for constitutive smUox expression (**f**). Quantitative morphometric analysis revealed 3.3% ± 2.9 (s.d.)/1.5% ± 0.8 (s.d.) (**c**), 109.1% ± 27.3 (s.d.)/26.9% ± 5.6 (s.d.) (**d**), 10.4% ± 4.6(s.d.)/3.7% ± 1.5 (s.d.) (**e**) and 0.4% ± 0.5 (s.d.)/0.6% ± 0.7 (s.d.) (**f**), percent crystals/percent relative area of crystalline deposits per tubulus and/or tubulus lumen profile of the respective treatment group. Scale bars, 100 µm.

and protein damage, mitochondrial dysfunction[22,23] and diseases such as cancer[24] and neurodegenerative disorders[22,25,26]. Uric acid should therefore be carefully regulated to balance its positive and negative physiologic effects[25].

Two urate-reducing drug classes have been developed for the treatment of chronic gouty arthritis[9]. Uricosuric drugs such as probenecid (Probenecid), losartan (Hyzaar) and benzbromarone inhibit URAT1, thereby preventing reabsorption and increasing uric acid excretion. Xanthine oxidase inhibitors, such as allopurinol, oxypurinol (Oxyprim) and Febuxostat (Uloric)[27], which has recently been licensed by the US Food and Drug Administration for the treatment of chronic hyperuricemia, block metabolic production of uric acid. Xanthine oxidase inhibitors are used as first-line treatment of patients with renal calculi, renal insufficiency, urate overproduction and patients receiving simultaneous diuretic and cyclosporin therapies. In contrast, uricosuric drugs provide the treatment of choice in allopurinol-allergic patients and underexcretors with normal renal function and no history of urolithiasis. Cell implants harboring a UREX-based network are prosthetic devices which provide self-sufficient and reversible control of uric acid levels in the bloodstream by preventing critical urate accumulation while also preserving basal uric acid levels that may improve urate-based protection from oxidative stress. Such devices may therefore be equally suited as a preventive treatment and as a therapy for acute hyperuricemic disorders including the tumor lysis syndrome and gout.

By functionally assembling a human urate transporter, a hucO-HucR–derived sensor circuit and sensor-controlled expression of a secretion-engineered version of a clinically licensed *A. flavus* urate oxidase (or uricase) we have designed a synthetic mammalian uric acid homeostasis network that enables (i) monitoring of urate levels in the blood, (ii) automatic induction of the core sensor unit at pathologic urate levels, (iii) prompt reduction of urate by sensor-controlled expression of clinically licensed urate oxidase and (iv) spontaneous shutdown when physiologic urate levels have been reached. UREX-based control of urate levels in urate oxidase–deficient mice, which develop hyperuricemia with human-like symptoms[19], showed that the synthetic circuit operated as expected and most importantly within the clinically relevant concentration range.

In humans, formation of monosodium urate crystals leading to painful inflammations typically occurs at blood urate levels of above 6.8 mg/dl[11,23,24]. The crystals are known to dissolve at a circulation level below 6 mg/dl[9], and cure of chronic hyperuricemia would require long-term maintenance of serum urate levels below this level. The UREX sensor is able to sense such pathologic levels and trigger dose-dependent expression of secreted uricase, which consequently reduces urate in the bloodstream of treated animals to 5 mg/dl.

The simple design principle of this therapeutic circuit may motivate the assembly of other prosthetic networks that sense metabolic disturbances and circulating pathologic metabolites, process such signals and coordinate an adjusted therapeutic response. Provided that prosthetic networks are robust and operate in safely contained cell implants that can be readily replaced at reasonable intervals, such technology might provide standard preventive surveillance as well as precise interventions in acute situations.

METHODS

Methods and any associated references are available in the online version of the paper at http://www.nature.com/naturebiotechnology/.

Note: Supplementary information is available on the Nature Biotechnology website.

ACKNOWLEDGMENTS

We thank W. Weber (Albert-Ludwigs-Universität Freiburg, Germany) for conceptual input and for providing pBluescript-mHucR, M. Gilet for skillful assistance with the animal study and Marcia Schoenberg for critical comments on the manuscript. This work was supported by the Swiss National Science Foundation (grant no. 31003A-126022) and in part by the EC Framework 7 (Persist).

AUTHOR CONTRIBUTIONS

C.K., J.S. and M.F. designed the project, analyzed results and wrote the manuscript. C.K., M.G., M.D.-E.B. and V.D. performed the experimental work. J.S. designed the mathematical model and performed simulations.

COMPETING FINANCIAL INTERESTS

The authors declare no competing financial interests.

Published online at http://www.nature.com/naturebiotechnology/.
Reprints and permissions information is available online at http://npg.nature.com/reprintsandpermissions/.

© 2010 Nature America, Inc. All rights reserved.

1. Kramer, B.P. & Fussenegger, M. Hysteresis in a synthetic mammalian gene network. *Proc. Natl. Acad. Sci. USA* **102**, 9517–9522 (2005).
2. Kramer, B.P. *et al.* An engineered epigenetic transgene switch in mammalian cells. *Nat. Biotechnol.* **22**, 867–870 (2004).
3. Fussenegger, M. Synthetic biology: Synchronized bacterial clocks. *Nature* **463**, 301–302 (2010).
4. Tigges, M., Marquez-Lago, T.T., Stelling, J. & Fussenegger, M. A tunable synthetic mammalian oscillator. *Nature* **457**, 309–312 (2009).
5. Rinaudo, K. *et al.* A universal RNAi-based logic evaluator that operates in mammalian cells. *Nat. Biotechnol.* **25**, 795–801 (2007).
6. Weber, W., Daoud-El Baba, M. & Fussenegger, M. Synthetic ecosystems based on airborne inter- and intrakingdom communication. *Proc. Natl. Acad. Sci. USA* **104**, 10435–10440 (2007).
7. Dean, J.T. *et al.* Resistance to diet-induced obesity in mice with synthetic glyoxylate shunt. *Cell Metab.* **9**, 525–536 (2009).
8. Cairo, M.S. & Bishop, M. Tumour lysis syndrome: new therapeutic strategies and classification. *Br. J. Haematol.* **127**, 3–11 (2004).
9. Terkeltaub, R.A. Clinical practice. Gout. *N. Engl. J. Med.* **349**, 1647–1655 (2003).
10. Liebman, S.E., Taylor, J.G. & Bushinsky, D.A. Uric acid nephrolithiasis. *Curr. Rheumatol. Rep.* **9**, 251–257 (2007).
11. Terkeltaub, R., Bushinsky, D.A. & Becker, M.A. Recent developments in our understanding of the renal basis of hyperuricemia and the development of novel antihyperuricemic therapeutics. *Arthritis Res. Ther.* **8**, S4 (2006).
12. Daly, M.J. A new perspective on radiation resistance based on *Deinococcus radiodurans*. *Nat. Rev. Microbiol.* **7**, 237–245 (2009).
13. Wilkinson, S.P. & Grove, A. HucR, a novel uric acid-responsive member of the MarR family of transcriptional regulators from *Deinococcus radiodurans*. *J. Biol. Chem.* **279**, 51442–51450 (2004).
14. Wilkinson, S.P. & Grove, A. Negative cooperativity of uric acid binding to the transcriptional regulator HucR from *Deinococcus radiodurans*. *J. Mol. Biol.* **350**, 617–630 (2005).
15. Bellefroid, E.J., Poncelet, D.A., Lecocq, P.J., Revelant, O. & Martial, J.A. The evolutionarily conserved Kruppel-associated box domain defines a subfamily of eukaryotic multifingered proteins. *Proc. Natl. Acad. Sci. USA* **88**, 3608–3612 (1991).
16. Deans, T.L., Cantor, C.R. & Collins, J.J. A tunable genetic switch based on RNAi and repressor proteins for regulating gene expression in mammalian cells. *Cell* **130**, 363–372 (2007).
17. Oda, M., Satta, Y., Takenaka, O. & Takahata, N. Loss of urate oxidase activity in hominoids and its evolutionary implications. *Mol. Biol. Evol.* **19**, 640–653 (2002).
18. Enomoto, A. *et al.* Molecular identification of a renal urate anion exchanger that regulates blood urate levels. *Nature* **417**, 447–452 (2002).
19. Wu, X. *et al.* Hyperuricemia and urate nephropathy in urate oxidase-deficient mice. *Proc. Natl. Acad. Sci. USA* **91**, 742–746 (1994).
20. Legoux, R. *et al.* Cloning and expression in *Escherichia coli* of the gene encoding Aspergillus flavus urate oxidase. *J. Biol. Chem.* **267**, 8565–8570 (1992).
21. Fluri, D.A., Kemmer, C., Daoud-El Baba, M. & Fussenegger, M. A novel system for trigger-controlled drug release from polymer capsules. *J. Control. Release* **131**, 211–219 (2008).
22. Pacher, P., Beckman, J.S. & Liaudet, L. Nitric oxide and peroxynitrite in health and disease. *Physiol. Rev.* **87**, 315–424 (2007).
23. Whiteman, M. & Halliwell, B. Protection against peroxynitrite-dependent tyrosine nitration and alpha 1-antiproteinase inactivation by ascorbic acid. A comparison with other biological antioxidants. *Free Radic. Res.* **25**, 275–283 (1996).
24. Ames, B.N., Cathcart, R., Schwiers, E. & Hochstein, P. Uric acid provides an antioxidant defense in humans against oxidant- and radical-caused aging and cancer: a hypothesis. *Proc. Natl. Acad. Sci. USA* **78**, 6858–6862 (1981).
25. Kutzing, M.K. & Firestein, B.L. Altered uric acid levels and disease states. *J. Pharmacol. Exp. Ther.* **324**, 1–7 (2008).
26. Schwarzschild, M.A. *et al.* Serum urate as a predictor of clinical and radiographic progression in Parkinson disease. *Arch. Neurol.* **65**, 716–723 (2008).
27. Schumacher, H.R. Jr., Becker, M.A., Lloyd, E., MacDonald, P.A. & Lademacher, C. Febuxostat in the treatment of gout: 5-yr findings of the FOCUS efficacy and safety study. *Rheumatology (Oxford)* **48**, 188–194 (2009).

© 2010 Nature America, Inc. All rights reserved.

ONLINE METHODS

Vector construction. Design details of all plasmids and oligonucleotides are provided in **Supplementary Table 1**.

Cell culture and transfections. HeLa (American Type Culture Collection (ATCC)), HEK-293 (ATCC) and HT-1080 (ATCC) were cultivated in DMEM (Invitrogen) supplemented with 10% (vol/vol) FCS (PAN Biotech) and 1% (vol/vol) penicillin/streptomycin solution (P/S, PAN Biotech). All cell types were cultivated at 37 °C in a humidified atmosphere containing 5% CO_2. HEK-293 were transfected using a standard $CaPO_4$-based protocol[2]. HeLa were also transfected according to this standard $CaPO_4$-based protocol, with the exception that the DNA precipitates were incubated with the cells for 12 h before changing the medium. HT-1080 were transfected with FuGENE 6 (Roche Diagnostics) according to the supplier's procedure. Transfected cells were cultivated in DMEM supplemented with 10% (vol/vol) knockout serum replacement (KOSR, Invitrogen), 1% P/S and, optionally, with uric acid (Acros Organics) (standard medium). Transgene expression values were normalized for variations in transfection efficiency by parallel transfections using the constitutive EYFP-expression vector pDF60. To establish uric acid-dependent dose-response characteristics, 3×10^5 cells were seeded per well of a six-well plate (Thermo Fisher Scientific) and transfected as described above. The cells were trypsinized (200 µl trypsin; PAN Biotech; 5 min, 37 °C), collected by centrifugation (2 min, 120*g*) and resuspended in 1.5 ml standard medium. We transferred 100 µl of this cell suspension to individual wells of a 96-well plate, supplemented cells with different concentrations of uric acid and cultivated them for 48 h before reporter gene expression was profiled in the culture supernatant.

Semiquantitative RT-PCR. 1 µg of total cellular RNA, isolated from mock-, pURAT1-, pOAT2-, or pCK65 and pCK25 transfected HeLaURAT1, HEK-293 and HT-1080 cells using the RNeasy Mini Kit (Qiagen), was reverse transcribed using the TaqMan Reverse Transcription Reagents (Applied Biosystems) and the RNA levels were quantified with the Mastercycler ep gradient/S system (Vaudaux-Eppendorf) and probes specific for URAT1, OAT2, smUox and the glyceraldehyde-3-phosphate dehydrogenase (GAPDH) (**Supplementary Table 2**).

Analytical assays. SEAP levels were quantified in cell culture supernatants and mouse serum using a standard *p*-nitrophenylphosphate-based light-absorbance time course[2,6]. Uric acid levels were assessed in cell culture supernatants, murine serum or urine using the Amplex Red uric acid/uricase assay kit (Invitrogen) according to the manufacturer's protocol. In brief, uric acid–containing samples were diluted in reaction buffer. The addition of uricase triggered the enzymatic conversion of uric acid to allantoin, CO_2 and H_2O_2, which reacts, in the presence of horseradish peroxidase stoichiometrically with Amplex Red reagent to generate the red-fluorescent oxidation product resorufin, which can be quantified at 585 nm.

Construction of stable transgenic cell lines. HeLa-derived $HeLa_{URAT1}$ cells, transgenic for the constitutive expression of the human renal urate-anion exchanger (URAT1), were constructed by co-transfection of pURAT1 (P_{hCMV}-URAT1-pA; ImaGenes) and pZeoSV2 (conferring resistance to zeocin; Invitrogen) at a ratio of 10:1. After a 14-d selection period using 200 µg/ml (wt/vol) zeocin cells were clonally expanded and individual clones were profiled for URAT1 expression using qRT-PCR. The cell line $HeLa_{URAT1}$ was chosen for further experiments. The triple-transgenic HEK-293–derived $HEK\text{-}293_{UREX15}$ cell line, enabling urate-inducible SEAP expression, was constructed by sequential co-transfection and clonal selection of (i) pCK9 (P_{UREX8}-SEAP-pA) and pCK25 ($P_{hEF1\alpha}$-KRAB-mHucR-pA, also carrying a constitutive expression cassette conferring resistance to blasticidin) (ratio of 1:1, 14-d selection in DMEM containing 10% FCS and 20 µg/ml (wt/vol) blasticidin (InvivoGen)) and (ii) pURAT1 (P_{hCMV}-URAT1-pA) and pZeoSV2 (conferring resistance to zeocin) (ratio of 10:1, 14-d selection in DMEM containing 10% FCS, 20 µg/ml (wt/vol) blasticidin and 200 µg/ml (wt/vol) zeocin (InvivoGen). Individual $HEK\text{-}293_{UREX}$ clones were randomly picked and assessed for urate-triggered SEAP expression. $HEK\text{-}293_{UREX15}$ was chosen for further studies.

***In vivo* methods.** Urate oxidase-deficient mice ($uox^{-/-}$) developing hyperuricemia with human-like symptoms[19] were used to validate the synthetic UREX-based uric acid control network *in vivo* (Charles River Laboratories). Because $uox^{-/-}$ mice die within 4 weeks of age, breeding and long-term maintenance requires the addition of 150 µg/ml (wt/vol) allopurinol (Sigma) to the drinking water[19]. Two weeks before implantation of UREX-transgenic cells the allopurinol treatment of urate oxidase–deficient mice was either continued or stopped to produce animal groups with low or high pathogenic uric acid levels in the bloodstream, respectively. $HeLa_{URAT1}$ mice, transgenic for constitutive URAT1 expression, were either transiently transfected with pCK65 to provide an isogenic constitutive smUox expression control or co-transfected with pCK25 and either pCK9, pSEAP2-control or pCK65 and then microencapsulated in 200 µm alginate-(poly-L-lysine)-alginate capsules (200 cells/capsule) using an Inotech Encapsulator Research IE-50R (EncapBioSystems), according to the manufacturer's protocol and applying the following settings: 200 µm single nozzle, stirrer speed control set to 5 units, 20-ml syringe with a flow rate of 410 units, nozzle vibration frequency 1,024 Hz, voltage for capsule dispersion 900 V. 700 µl PBS containing 2×10^6 encapsulated cells (10^4 capsules/mouse) was intraperitoneally injected into urate oxidase–deficient mice. Control mice were implanted with microencapsulated parental $HeLa_{URAT1}$. Two and 6 d after implantation, the mice were transferred to a clean cage and the urine of each treatment group was sampled for 24 h. Three and 7 d after implantation the mice were euthanized, their blood was collected and the serum isolated in microtainer SST tubes (Becton Dickinson) according to the manufacturer's protocol. All experiments involving animals were performed according to the directive of the European Community Council (86/609/EEC), approved by the French Republic (no. 69266310) and carried out by M.D.E. at the Institut Universitaire de Technologie, IUTA, F-69622 Villeurbanne Cedex, France.

Mathematical modeling. All details on model development are provided in the **Supplementary Results**, **Supplementary Figures 2–13** and **Supplementary Tables 3–6**.

Histology and quantification of uric acid crystals in renal tubules. For microscopic analysis of uric acid crystal deposits in the kidney of $uox^{-/-}$ mice implanted with microencapsulated cells transgenic for constitutive URAT1 and UREX-controlled smUox expression–treated animals were split into treatment groups receiving 150 µg/ml (wt/vol) or no allopurinol in their drinking water as described above. Seven days after implantation, the mice were euthanized, their kidneys explanted and fixed in 4% (wt/vol) paraformaldehyde (Sigma) in PBS for 4 h. The kidneys were washed in 10% (wt/vol) sucrose (Sigma) in PBS for 90 min, trimmed, dehydrated and embedded in paraffin. An ultracut device (Zeiss) was used to obtain 3-µm sections of the tissues, which were transferred to gelatinized microslides and air-dried overnight at 37 °C. After paraffin removal by submersion in xylene (3×10 min), the tissues were rehydrated by sequential incubation (10 min) in decreasing ethanol concentrations (90%, 80%, 70%), rinsed twice in TBS (Tris-buffered saline; 50 mM Tris/HCl (pH 7.4), 100 mM NaCl) and stained with H&E solution. The samples were visualized under polarized light to assess anisotropism using a Leica DMRBE microscope. The number of crystals as well as the total crystalline area of kidney sections, derived from at least five animals per treatment group, was quantified using the iTEM morphometry software (Olympus Soft Imaging Solutions).

© 2010 Nature America, Inc. All rights reserved.